

# Towards seasonal sea ice predictions for the Arctic based on assimilation of remotely sensed observations

F. Kauker<sup>1,3</sup>, T. Kaminski<sup>2,\*</sup>, R. Ricker<sup>3</sup>, L. Toudal-Pedersen<sup>4</sup>, G. Dybkjaer<sup>4</sup>,  
C. Melsheimer<sup>5</sup>, S. Eastwood<sup>6</sup>, H. Sumata<sup>3</sup>, M. Karcher<sup>1,3</sup>, and R. Gerdes<sup>3,7</sup>

<sup>1</sup>OASys, Tewssteg 4, 20249 Hamburg, Germany

<sup>2</sup>The Inversion Lab, Tewssteg 4, 20249 Hamburg, Germany

<sup>3</sup>Alfred Wegener Institute, Bussestr. 24, 27570 Bremerhaven, Germany

<sup>4</sup>Danish Meteorological Institute, Lyngbyvej 100, 2100 Copenhagen, Denmark

<sup>5</sup>University of Bremen, Institute for Environmental Physics, Otto-Hahn-Allee 1, 28359 Bremen, Germany

<sup>6</sup>The Norwegian Meteorological Institute, Blindern 43, 0313 Oslo, Norway

<sup>7</sup>Jacobs University, Campus Ring 1, 28759 Bremen, Germany

\*previously at FastOpt

*Correspondence to:* F. Kauker (frank@OASys-research.com)

**Abstract.** The recent thinning and shrinking of the Arctic sea ice cover has increased the interest in seasonal sea ice forecasts. Typical tools for such forecasts are numerical models of the coupled ocean sea ice system such as the North Atlantic/Arctic Ocean Sea Ice Model (NAOSIM). The model uses as input the initial state of the system and the atmospheric boundary condition over the forecasting period. This study investigates the potential of remotely sensed ice thickness observations in constraining the initial model state. For this purpose it employs a variational assimilation system around NAOSIM and the Alfred Wegener Institute's CryoSat-2 ice thickness product in conjunction with the University of Bremen's snow depth product and the OSI SAF ice concentration and sea surface temperature products. We investigate the skill of predictions of the summer ice conditions starting in March for three different years. **combines, for the first time, remotely sensed observations of four variables of the ocean sea ice system in a data assimilation system. The four data streams are the Alfred Wegener Institute's CryoSat-2 ice thickness product, the University of Bremen's snow depth product, and the OSI SAF ice concentration and sea surface temperature products. The assimilation system, built around NAOSIM, uses a variational approach with a two-month assimilation window, in which all observations act simultaneously as constraints on the initial model state.** We investigate the skill of predictions of the summer ice conditions issued in ~~March~~ **May** for three different years. Straightforward assimilation of the above combination of data streams results in slight improvements over some regions (especially in the Beaufort Sea) but degrades the over-all fit to independent observations. A considerable enhancement of forecast skill

20 is demonstrated for a bias correction scheme for the CryoSat-2 ice thickness product that uses a spatially varying scaling factor.

## 1 Introduction

The state of the Arctic climate system is rapidly changing (Stroeve et al., 2007). This change is impacting ecosystems, coastal communities, and economic activities. In this context, high-quality predictions of the ice conditions are of paramount interest (AMAP, 2011). This topic is addressed, for example, by the Sea Ice Outlook (<http://www.arcus.org/sipn/sea-ice-outlook>). In this activity, various research groups are applying different approaches to predict the Arctic summer minimum sea ice extent based on the state of the Arctic system at the beginning of the melting season (around May/June). The range of approaches extends from heuristic techniques, statistical models, coupled sea ice ocean models to fully coupled models of the atmosphere sea ice ocean system. An analysis of Stroeve et al. (2014) shows that none of the approaches outperforms its competitors. In general, however, due to the rapid transition of the Arctic system, the validity of heuristic and statistical relationships derived from the past may be limited (Holland and Stroeve, 2011). In contrast, dynamical models that include all relevant processes should be able to handle such transitions although the values of their process parameters are based on past observations. While some of the dynamical models (fully coupled models) include an atmospheric component (see, e.g. Wang et al. (2013); Chevallier et al. (2013); Sigmond et al. (2013)), other models are restricted to the ocean sea ice system (ocean sea ice models, see, e.g. Zhang et al. (2008); Lindsay et al. (2012); Massonnet et al. (2015)). The latter class of models are driven with prescribed atmospheric fields, provided, e.g., by atmospheric forecasting/numerical weather prediction centres. These fields are typically constrained by a range of atmospheric observations and are thus probably more realistic than those computed by a fully coupled model. On the other hand, fully coupled models allow a consistent simulation of the feedback loops through all components of the atmosphere-sea ice-ocean system.

**The potential for sea-ice predictions has been addressed by a set of studies (e.g. Kauker et al. (2009); Koenigk and Mikolajewicz (2009); Holland et al. (2010); Day et al. (2014)).** Predictions by a dynamical model depend on the state of the system at the beginning of the simulation period (initial state). Previous studies have highlighted the role of the initial ice thickness distribution (Kauker et al., 2009; Holland and Stroeve, 2011; Lindsay et al., 2012; Chevallier and Salas-Méla, 2012) for the forecast quality. Systematic use of observational information in a data assimilation system can help to derive an improved estimate of the initial state (Lindsay et al., 2012; Chevallier et al., 2013; Yang et al., 2014; Massonnet et al., 2015).

The present article describes the ~~construction~~ **development** of an assimilation and prediction system of the Arctic sea ice conditions. ~~Observational data streams for such a prediction system have to be available near real time. We use four data streams which fulfill this requirement,~~ **Ideally, such a system will combine with a numerical model with observational data of various types, for example in terms of variables (e.g. sea ice or ocean), scale of representativeness (e.g. point or two dimensional area), or observational approach (e.g. in-situ or satellite-derived). We term each of these types a data stream, and for the use in a combined assimilation/prediction sys-**

tem, an obvious requirement is their availability close to near real time. In this study, we use  
60 **four data streams which fulfill this requirement**, namely, the OSI SAF sea ice concentration and  
sea surface temperature products, a snow depth product provided by the University of Bremen, and  
the CryoSat-2 ice thickness product derived at the Alfred Wegener Institute (AWI). **All above data  
streams are available from 2012.** The availability of the above data streams is limited to the period  
from 2012 to 2014. Also there is only one single two month period per year (March and April) for  
65 which the CryoSat-2 product is currently available (and note that the followup version covers Oc-  
tober to April/May). We thus restrict our study to assimilation of the above four data streams in the  
spring of each of the three years **from 2012 to 2014** and to prediction of the ice conditions in the  
following summer.

The assimilation system is built around the regional North Atlantic/Arctic Ocean Sea Ice Model  
70 (NAOSIM, Gerdes et al. (2003), Kauker et al. (2003)). Initial tests indicated that the model was not  
sufficiently calibrated to achieve the required high simulation quality. Hence, in a preliminary step,  
some of the process parameters in the formulation of our model were adapted to better match obser-  
vations over the 19 year period from 1990-2008. Furthermore, it turned out that the assimilation sys-  
tem was not capable of integrating the information in the above mentioned CryoSat-2 ice thickness  
75 product to a sufficient degree. Through a set of additional assimilation experiments, we were able to  
develop a so-called bias correction scheme that allowed to take full advantage of this data stream. We  
**apply a variational assimilation approach that determines an initial state (of sea-ice and ocean  
fields) on March 1. This means through variation of the model state on March 1 we search  
a trajectory that provides the best match to the four data streams over a subsequent two-  
80 month interval (assimilation window). The seasonal forecast is then performed by a simulation  
from that initial state along that trajectory into the future. Moving on a model trajectory  
means that we simulate a temporal sequence of states that fulfills the dynamical constraints  
imposed by the equations governing the model, including the fundamental conservation laws  
of mass, momentum, and energy. In summary, all observational information in the two-month  
85 observation window is used to constrain the initial state on March 1. All subsequent changes  
to model variables (including the forecast) are consequences of the constrained initial state.**

It is evident that this approach has the potential to reveal inconsistencies between the model  
and our four data streams that otherwise would remain undetected. Such an inconsistency  
could be, for example, a huge ice thickness in a grid cell with little ice concentration. It could  
90 yield to some combination of a bad match of the observations, an unrealistic initial state, and  
an unrealistic forecast. Exactly this type of inconsistencies were detected in initial preparatory  
experiments. Hence, a first part of this study attempts to minimise biases by adapting some of  
the process parameters in the formulation of our model to better match observations over the  
19 year period from 1990-2008. To evaluate the success of this calibration exercise we compare  
95 the calibrated model with two independent models that are typically used as reference.

A second part of the study pursues a series assimilation experiments with our calibrated model and the four data streams. The first set of experiments still reveals inconsistencies which becomes evident through a low forecast skill for summer ice concentration. A second set of assimilation experiments (without the ice thickness data stream), enables us to develop a so-called bias correction scheme. Integrating this bias correction scheme into the assimilation scheme results in a substantially enhanced forecast skill for summer ice concentration as demonstrated by a final set of experiments.

## 2 Methods

### 2.1 Assimilation

NAOSIMDAS is a variational assimilation system that estimates a control vector  $x$  through minimisation of a cost function  $J(x)$  that quantifies the fit to all observations plus the deviation from prior knowledge on  $x$ . A coupled ocean sea ice model computes a sequence of states of the ocean sea ice system (trajectory) from an initial state. By varying the initial state we can control the trajectory along which the model evolves. Thus we denote the vector composed of all initial model fields as control vector,  $x$ . The task of a variational assimilation is to minimise the difference of the model simulation to the available set of observations,  $d$ . This observation vector is typically a subset of all variables that can be simulated with the model at any point in time (within a given assimilation window) and space (within the model domain). To formalise the assimilation methodology it is useful to consider the model as a mathematical mapping (function)  $M(x)$  from the control vector to the observation vector, more precisely to its equivalent simulated with the model. The assimilation system seeks a control vector,  $x_{post}$  such that  $M(x_{post})$  achieves the best possible match to the observation vector  $d$ . At the same time we want to use any extra information we already have on  $x$ , the so-called prior information  $x_0$ . As the information on the model, the observations, and the prior is only approximate the theory is most conveniently formulated in terms of probability density functions (PDFs) (Tarantola, 2005). For computational convenience one typically assumes Gaussian distributions of the prior and the observations and can then show that  $x_{post}$  minimises the following cost function:

$$J(\mathbf{x}) = \frac{1}{2} \left[ (M(\mathbf{x}) - \mathbf{d})^T \mathbf{C}(d)^{-1} (M(\mathbf{x}) - \mathbf{d}) + (\mathbf{x} - \mathbf{x}_0)^T \mathbf{C}(x_0)^{-1} (\mathbf{x} - \mathbf{x}_0) \right] \quad (1)$$

where  $M$  denotes the model, considered as a mapping from the control vector to observations,  $d$  the observations with data uncertainty covariance matrix  $\mathbf{C}(d)$ ,  $x_0$  the vector of prior values of the control variables with uncertainty covariance matrix  $\mathbf{C}(x_0)$ , and the superscript  $T$  is the transposed. The control variables are typically a combination of the initial state, the atmospheric forcing and the process parameters. In this study the control vector is restricted to the model's initial state. where

$\mathbf{C}(x_0)$  denotes the uncertainty covariance matrix of the prior and the superscript  $T$  is the  
 130 **transposed.**

The data uncertainty  $\mathbf{C}(d)$  reflects the combined effect of observational  $\mathbf{C}(d_{\text{obs}})$  and model error  
 $\mathbf{C}(d_{\text{mod}})$  :

$$\mathbf{C}(d)^2 = \mathbf{C}(d_{\text{obs}})^2 + \mathbf{C}(d_{\text{mod}})^2 \quad (2)$$

$\mathbf{C}(d_{\text{mod}})$  captures all uncertainty in the simulation of the observations except for the uncertainty in  
 135 the control vector, because this fraction of the uncertainty is explicitly addressed by the assimilation  
 procedure through correction of the control vector. In this study we assume that  $\mathbf{C}(d_{\text{obs}})$  considerably  
 exceeds  $\mathbf{C}(d_{\text{mod}})$  and neglect the latter. The non-diagonal elements of  $\mathbf{C}(d_{\text{obs}})$  are assumed to be zero  
 (no correlation of the uncertainty of different components of the observation vector). The same is  
 assumed for the prior uncertainty,  $\mathbf{C}(x_0)$ . **This means equation (1) reduces to**

$$140 \quad J(\mathbf{x}) = \frac{1}{2} \sum_j \left( \frac{M_j(\mathbf{x}) - d_j}{\sigma(d_{\text{obs},j})} \right)^2 + \frac{1}{2} \sum_i \left( \frac{x_i - x_{0,i}}{\sigma(x_{0,i})} \right)^2, \quad (3)$$

where  $i$  counts the components of  $x$  and  $j$  the components of  $d$ .

The prior information on the initial state is taken from a preceding model run without assim-  
 145 **ilation (described in section 2.3). The prior term in the cost function achieves a regularisation,**  
**i.e. it determines  $x_{\text{post}}$  in a (hypothetical) case of an element of the control vector to which none**  
**of the observations is sensitive.**

Our assimilation approach is specifically tailored to seasonal forecasting of sea ice conditions  
 with a coupled ocean sea ice model. It is not taken out of the shelf and thus does not fit in the  
 classification of data assimilation methods used in numerical weather prediction (NWP), the  
 pioneering domain of data assimilation. It is a variational approach that assures consistency  
 150 **with the model equations (respecting the fundamental conservation laws) over the entire assim-**  
**ilation window. This is contrasted by sequential approaches which partition the assimilation**  
**window into sub-intervals, for each of which they perturb the model state (violating conserva-**  
**tion laws) to better match the observations in that sub-interval. As NWP is confronted with a**  
**limit of predictability in the order of days (Lorenz, 1963), the typical NWP assimilation window**  
 155 **(even when using the so-called four dimensional variational assimilation approach) is a day or**  
**less, i.e. the dynamical consistency is only assured over this short period of time (plus the sub-**  
**sequent forecast period). Consistency with observations over a longer time period is achieved**  
**by a sequence of assimilation runs, each resulting in a perturbation of the state. It is important**  
**to note that, by contrast, our long time window assures dynamical consistency for the entire**  
 160 **two month assimilation window plus the subsequent forecasting period. The closest relative to**  
**our approach in the classical NWP taxonomy is perhaps "long time window four dimensional**  
**variational assimilation". We note that, for other applications, we operate NAOSIMDAS with**

**an extended control vector that also includes boundary conditions (e.g. surface wind or air temperature) or model process parameters.**

165 Technically, the cost function is minimised by a gradient algorithm. The algorithm iteratively uses the gradient of the cost function **with respect to the control vector**, which is efficiently provided by so-called adjoint code of NAOSIM (Kauker et al., 2009) generated by the automatic differentiation tool TAF (Giering and Kaminski, 1998).

## 2.2 Observations

170 This study assesses the potential of remotely sensed observations of the sea ice and ocean system to increase the skill of seasonal predictions of that system through initialisation of NAOSIM. For this purpose, the data streams have to be available operationally or have to become operational in the near future, **i.e. the product time series need to be continuously extended until the recent past (near real time)**. EUMETSAT's Ocean and Sea Ice Satellite Application Facility (OSI SAF)  
175 operationally provides sea ice concentration and sea surface temperature. Currently available sea ice thickness products are derived from SMOS (Kaleschke et al., 2012) and CryoSat-2 (Wingham et al., 2006). While the SMOS product copes better with thin ice, CryoSat-2 copes better with thick ice. As thinner ice tends to be completely melted in summer, we expect the information on thicker ice to be more important in our context and select a CryoSat-2 product, namely the one provided by the  
180 Alfred Wegener Institute (Ricker et al., 2014). A snow depth product is provided by the University of Bremen. The above data sets allow to perform data assimilation experiments starting in March for each of the years 2012 to 2014 and will be described in more detail below.

As mentioned above, a preliminary step consists in the calibration of the model against observations (labeled historical) over the period from 1990-2008 (calibration period). Operational availabil-  
185 ity of the data products was obviously not required. We use remotely sensed sea ice concentration provided by OSI SAF, sea ice thickness from ICESat provided by JPL, and two drift products. A detailed description of the products is provided below.

### 2.2.1 Historical Data Sets

The only data stream available all year for the entire calibration period is the re-processed OSI SAF  
190 ice concentration product (Eastwood et al., 2015). It is available in daily temporal and 10 km spatial resolution and includes spatially and temporally varying uncertainty estimates  $\sigma(d_{\text{obs}})$  as required by equation (1).

The ICESat-JPL ice thickness (available in Feb/March and Oct/Nov from 2003 to 2008) is avail-  
195 able at about monthly temporal and 25 km spatial resolution and does not include an uncertainty estimate. Kwok and Cunningham (2008) estimate a mean error of about 50 cm, corresponding to a relative error of about 40%. For the present study we thus use 40% relative uncertainty but completely exclude observations below 1m (as the uncertainty increases for thin ice). ICESat-JPL thick-

ness data are omitted where the difference to the ICESat thickness product provided by the Goddard Space Flight Center (ICESat-GSFC, Zwally et al. (2008)) exceeds 40 cm.

200 The OSI SAF winter ice drift product (Lavergne et al., 2010) is available at bi-daily temporal and 62.5 km spatial resolution but does not include uncertainty estimates. In the present study we use the monthly mean value and corresponding uncertainty estimates of Sumata et al. (2014). This data set covers the winter season (October to April) for the period from October 2003 to December 2006.

205 The KIMURA summer ice drift product (Kimura et al., 2013) is available at daily temporal and 75 km spatial resolution and does not include uncertainty estimates either. As for the winter ice drift we use monthly mean values and uncertainty estimates derived by Sumata et al. (2015). The data set covers the summer months May to July for the years 2003 to 2007.

### 2.2.2 Operational Products

The operational OSI SAF ice concentration product is available at daily temporal and 10 km spatial  
210 resolution and based on the combination of the Comiso frequency mode (CF) algorithm and the Bristol (BR) algorithm. Both products use the 19 and 37 GHz channels, with respective native resolutions (footprints) of about 60 and 30 km. The product does include discrete quality flags (while the followup product will provide an uncertainty estimate). For this study an uncertainty estimate is derived by a procedure that was developed within the Sea Ice project (<http://esa-cci.nersc.no/>) of  
215 ESA's Climate Change Initiative (SICCI). The procedure considers the algorithmic uncertainty and a so-called 'smearing uncertainty'. The algorithmic uncertainty  $\sigma_a$ , i.e. the uncertainty derived by propagating radiometric noise through the algorithm, is only available in the re-processed OSI SAF concentration product. As it hardly exceeds 6 percentage points in the re-processed product, this value is used for all grid cells and all days as a conservative estimate of the algorithmic uncertainty.  
220 The (spatially and temporally variable) smearing uncertainty reflects the combination of two sources of error: first, the error caused by providing a 10 km product from coarser native resolutions, and, second, the error caused by combining channels with different footprints. An estimate of this uncertainty is calculated by comparing high resolution SIC aggregated to 10 km resolution (reference) and that computed at the SSMI footprints using both, the CF and the BR algorithm. The empirical  
225 formula  $\sigma_s = \sqrt{sd}/2.2$  (see Figure 1) provides an approximation of the root mean squared difference as a function of the 3x3 standard deviation  $sd$  (grid point and eight surrounding grid points). Assuming the independence of both uncertainties the total observational uncertainty is given by  $\sigma(d_{\text{obs}}) = \sqrt{\sigma_a^2 + \sigma_s^2}$ .

230 The OSI SAF high latitude SST product (Eastwood, 2011a) has a resolution of 5 km and is produced twice daily at 00 UTC and 12 UTC. It covers the Atlantic Ocean from 50N to 90N, with the exception of areas covered by ice or clouds. A constant uncertainty of 0.5K is applied (Eastwood, 2011b).

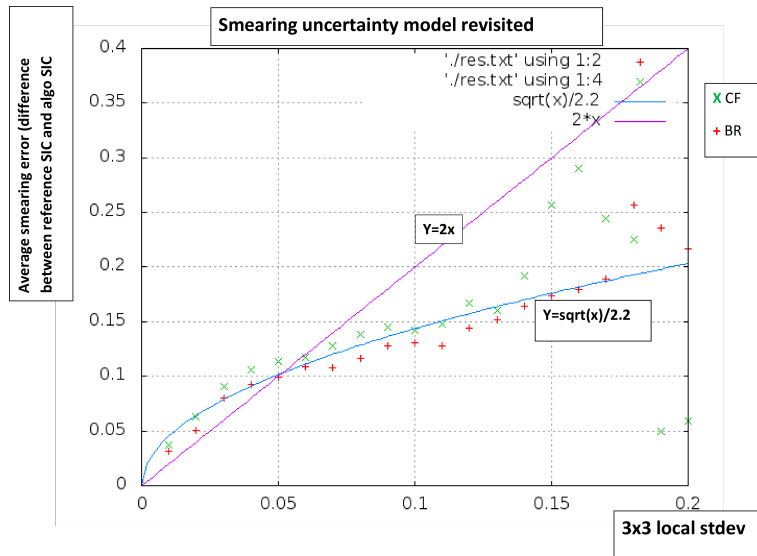


Figure 1: The empirical fit of the smearing uncertainty. Root mean squared difference between high resolution SIC aggregated to 10 km resolution (reference) and that computed at the SSMI footprints using the Comiso Frequency mode (CF, green crosses) or the BRistol (BR, red crosses) algorithms (which are applied in the OSISAF algorithm).

AWT's CryoSat-2 ice thickness product is provided on a monthly temporal and 25 km spatial grid, including an ice type classification into first-year and multi-year ice, which is adopted by the  
 235 OSI SAF ice type product (Eastwood et al., 2015). The main source of systematic uncertainty in the CryoSat-2 ice thickness retrieval is due to the selection of the return-power threshold value in the retracker algorithm (Ricker et al., 2014). This algorithm is essential to derive the actual range measurement from the radar-return signal. Therefore, a return-power threshold is used at the first maximum of the echo power distribution to retrieve the range estimate, which is then used to calculate sea ice thickness. In order to estimate this algorithm uncertainty, we use a small ensemble of ice thickness values retrieved by Ricker et al. (2014) for three different thresholds with 40, 50, and 80% (range of value in the literature) of the first maximum of the radar echo power. For the present study we use the ice thickness retrieved with the 50% threshold as it provides the best match to the ice thickness, simulated by (the recalibrated version of) NAOSIM. The standard deviation of  
 240 this ensemble over first-year ice is about 20% and over multi-year ice about 50%. We use these two values as relative uncertainties of the ice thickness for the respective ice types.

A snow depth product on the NAOSIM grid is provided by the University of Bremen on the model's grid. It has a daily temporal resolution and includes uncertainty estimates. The basis is an algorithm following Markus and Cavalieri (1998), which is applicable to level ice under non-melting  
 250 conditions. To mask out areas where these conditions are not met, the radar backscatter at 5.3 GHz (C band) is used as it is increased in melting conditions and for rough ice. Here, a threshold of  $-13\text{dB}$

for the normalised radar backscattering cross section is used. On first-year ice the maximum of the following three uncertainty estimates is used: (1) a value of 6 cm as estimated from a comparison with the NASA ice bridge mission (Kurtz et al., 2013a, b), (2) a value derived by Gaussian error propagation from the radiometric error of the input data (satellite brightness temperatures) and the uncertainty of the retrieval parameters, (3) the standard deviation of the most recent five days of retrieved snow depths. On multi-year ice and under melting-conditions a very large uncertainty of 5m is applied.

### 2.3 NAOSIM

NAOSIM is constructed around the North Atlantic/Arctic Ocean Sea Ice Model (NAOSIM) (Kauker et al., 2003). The **ocean** model is derived from version 2 of the Modular Ocean Model (MOM-2) of the Geophysical Fluid Dynamics Laboratory (GFDL). The version of NAOSIM used here has a horizontal grid spacing of  $0.5^\circ$  on a rotated spherical grid. The rotation maps the  $30^\circ W$  meridian onto the equator and the North Pole onto  $0^\circ E$ . In the vertical it resolves 20 levels, their spacing increasing with depth. The ocean model is coupled to a sea ice model with viscous-plastic rheology (Hibler, 1979). **The thermodynamics are formulated as a zero-layer model following Semtner (1976), and its parameters (e.g. albedos) are set in accordance to the AOMIP protocol (Nguyen et al., 2011). Freezing and melting are calculated by solving the energy budget equation for a single ice layer with a snow layer and an ocean mixed layer according to Parkinson et al. (1979). In contrast to the original formulation the energy flux through the ice is calculated by a PDF for the distribution of ice thickness based on EM-bird measurements (Castro-Morales et al., 2014). The sea ice model's prognostic variables are ice thickness, ice concentration, and snow depth. Ice drift is calculated diagnostically from the momentum balance. All quantities are mean quantities over a grid box. When atmospheric temperatures are below the freezing point, precipitation is added to the snow mass. The snow layer is advected jointly with the ice layer. The surface heat flux is calculated using prescribed atmospheric data and sea surface temperature predicted by the ocean model. The sea ice model is formulated on the ocean model grid and uses the same time step. The models are coupled following the procedure devised by Hibler and Bryan (1987).** At the open boundary near  $50^\circ N$  the barotropic oceanic transport is prescribed from a coarser resolution version of the model that covers the whole Atlantic north of  $20^\circ S$  (Köberle and Gerdes, 2003).

The state of the model comprises five fields, namely ocean temperature and salinity (velocities are diagnostic), ice thickness and concentration (drift is diagnostic) as well as snow depth. These five fields form the control vector  $x$  in our assimilation system described in section 2.1.

In contrast to the version described by Kauker et al. (2003), the present version uses a modified atmospheric forcing data set consisting of 10m-wind velocity, 2m-air temperature, 2m-specific humidity, total precipitation, and downward solar and thermal radiation. For the period from 1979 to

290 2010 the forcing is taken from the National Center for Environmental Prediction (NCEP) Climate Forecast System Reanalysis (NCEP-CFSR) (Saha et al., 2010) and for the period from 2011 to the end of 2014 from the NCEP Climate Forecast System version 2 (CFSv2) (Saha et al., 2014).

The initial state of January 1 1980 is taken from a hindcast from January 1 1948 to December 31 1979. As in Kauker et al. (2003) this hindcast run was forced by the NCEP/NCAR reanalyses (Kalnay et al., 1996) and, in turn, initialized from PHC (Steele et al., 2001) (ocean temperature and salinity), zero snow depth, and a constant ice thickness of 2m with 100% ice concentration where 295 the air temperature is below the freezing temperature of the ocean's top layer.

The above-described historical data sets were used to estimate a sub-set of the ocean sea ice model's process parameters, with focus on parameters that influence the ice dynamics. These are the atmospheric drag coefficient ( $cd_{air}$ ), the oceanic drag coefficient ( $cd_{wat}$ ), the ice strength parameter ( $p^*$ ), the parameter that determines the dependence of the ice pressure on the ice concentration ( $c^*$ ) 300 and the parameter that determines the ellipsoid of the rheology ( $eccen$ ) that represents the ratio of the normal stress and the shear stress. Additionally the vertical ocean tracer mixing parameter  $kappa_h$  is adjusted.

In our model we observe a memory of the Arctic sea ice system in the range of 7 to 10 years. We thus performed model runs over the 29 year period from January 1980 until end of December 2008, 305 skipped the first 10 years, and evaluated the (quasi) equilibrium response for the remaining 19 years (calibration period).

The performance of the model is evaluated in terms of its weighted fit (as defined by the first term of equation (3)) to observed sea ice concentration, ICESat-JPL ice thickness, winter ice drift from OSI SAF, and summer ice drift from KIMURA as described above (Table 1). For the computation of the total misfit, each ~~term~~ **data stream** is normalised to yield a value of 1 for the standard 310 configuration, in order to achieve an equal weighting of the terms despite their varying number of observations. By this procedure we find a configuration that reduces the misfit of ice thickness and ice drift strongly ~~but increases the misfit of ice concentration, especially in winter.~~ **The misfit of ice concentration is slightly decreased in summer but strongly increased in winter where the ice margin is located too far south.** Because here we are interested in the seasonal predictions of summer ice conditions, the deficit in winter can be tolerated. In the following we call this configuration newNAOSIM.

PIOMAS 2.1 (Zhang and Rothrock, 2003), an Arctic ocean sea ice model which uses Optimal Interpolation to assimilate ice concentration and sea surface temperature, is often used as a reference, 320 because it is well validated (see e.g. Schweiger et al. (2011)). Its misfit to ice thickness and ice drift is added to Table 1. NewNAOSIM performs slightly worse than PIOMAS2.1 with respect to ice thickness and better with respect to ice drift.

Another reference is TOPAZ4 (Sakov et al., 2012) which uses an Ensemble Kalman filter to assimilate satellite observed sea level anomaly, sea surface temperature, sea ice concentrations from

Model	concn.	concn.	ICESAT	ICESAT	drift	drift	total	weighted
	Nov-Apr	May-Oct	Feb/Mar	Oct/Nov	Oct-Apr	May-Jul		
NAOSIM	234429	430621	3550	3753	120959	126750	920063	3.00
newNAOSIM	405000	405221	1793	1664	22689	38131	963117	1.94
PIOMAS2.1	-	-	1383	1125	46231	67254	-	.
TOPAZ4	-	-	2949	2276	159021	109079	-	-

Table 1: The cost function for the three data streams separated by winter and summer (columns 2 to 7), the sum of the terms (column 8), and the normalized sum (column 9) for standard NAOSIM (NAOSIM) and the recalibrated NAOSIM (newNAOSIM). Additionally, the cost function with respect to the ICESAT thickness and ice drift is given for PIOMAS2.1 and TOPAZ4.

325 AMSR-E (NSIDC), sea ice drift products from CERSAT and Coriolis in-situ temperature and salinity profiles. NewNAOSIM outperforms TOPAZ4 with respect to ice thickness and ice drift (Table 1).

The deviations of the climatologies of newNAOSIM, PIOMAS2.1, and TOPAZ4 from the IceSat-JPL climatology (Figure 2) (from 2003 to 2008) reveal similarities between newNAOSIM and PIOMAS2.1 (compare Schweiger et al. (2011) figure 6). Both show too thick ice in the Beaufort Sea  
330 in February/March and too thin ice north of the Canadian Archipelago and north of Greenland and north of Fram Strait in February/March and October/November when compared to ICESat-JPL. This is very remarkable because both simulations differ in terms of model formulation and parameterisations and atmospheric forcing (NCEP-CFSR in case of NAOSIM and NCEP in case of PIOMAS2.1 which differ considerably for some variables, see e.g. Lindsay et al. (2014)). In contrast to new-  
335 NAOSIM and PIOMAS2.1 in February/March TOPAZ4 exhibits a large negative bias in the Eurasian Basin, especially north of Fram Strait. In October/November TOPAZ4 is closer to newNAOSIM and PIOMAS2.1. The ice thickness of newNAOSIM, PIOMAS2.1, and TOPAZ4 for September 2007 is shown in Figure 3. Although newNAOSIM uses no assimilation of sea ice or ocean observations the pattern of the sea ice cover deviates not stronger from PIOMAS2.1 and TOPAZ4 than PIOMAS2.1  
340 deviates from TOPAZ4 (although both models use assimilation of ice concentration from NSIDC).

The sea ice area in September for newNAOSIM is in good agreement with three different observational data streams (Figure 4). The minima in 2007 and 2013 and the long-term trend are captured by the model. The largest deviations occur between 1999 and 2003 where the model overestimates the sea ice area. As this strong deviation is absent when forced with the NCEP reanalysis (not shown)  
345 this can be attributed to deficits in the NCEP-CFSR surface forcing.

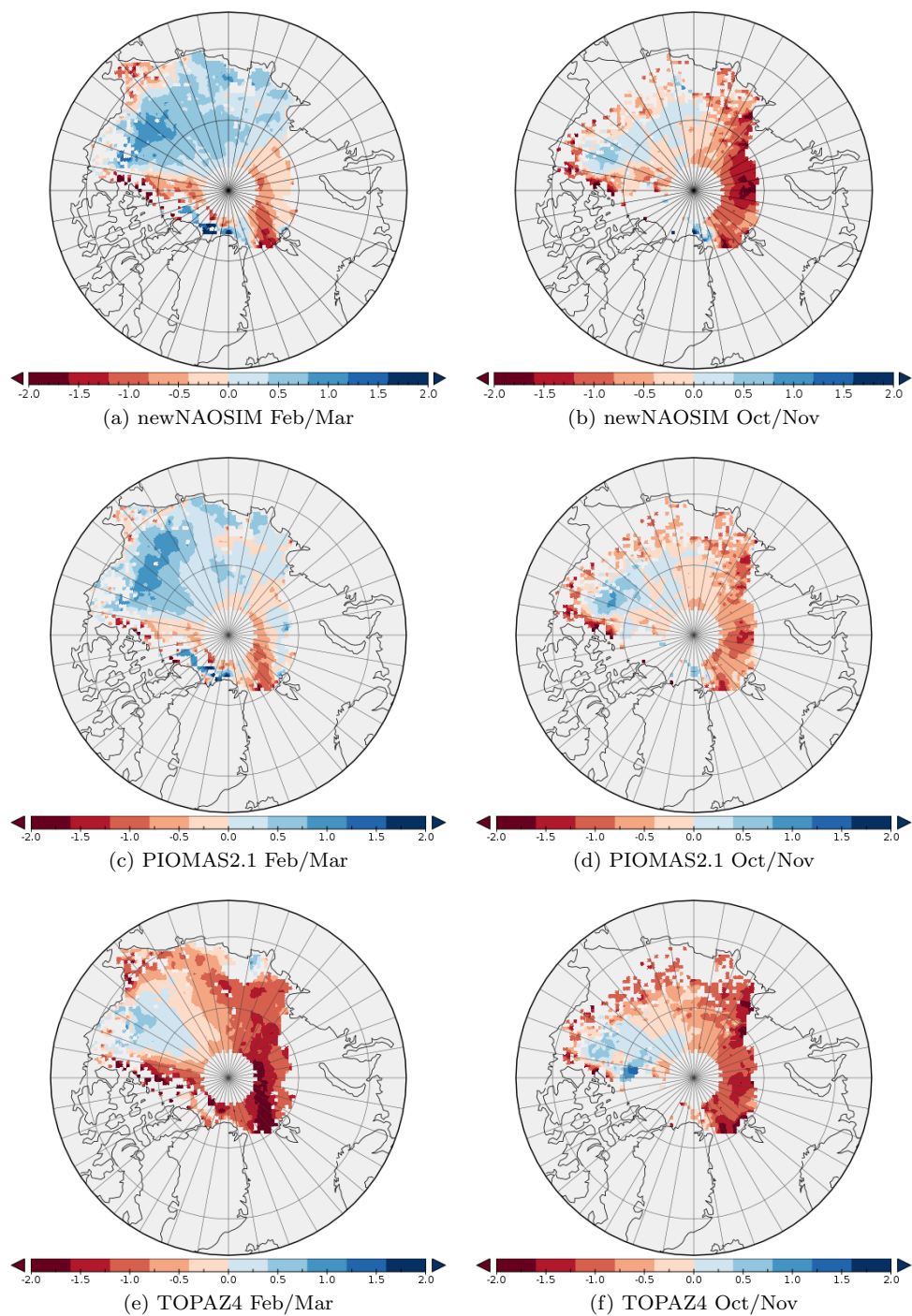


Figure 2: The difference of the modelled and observed (ICESat-JPL) ice thickness climatology [m] for February/March (left) and October/November for newNAOSIM (a) and b)), PIOMAS2.1 (c) and d)), and TOPAZ4 (e) and f)) for the mean from 2003-2008). Only points where the deviation of ICESat-JPL from ICESAT-GSFC (Zwally et al., 2008)) is below 40cm are used.

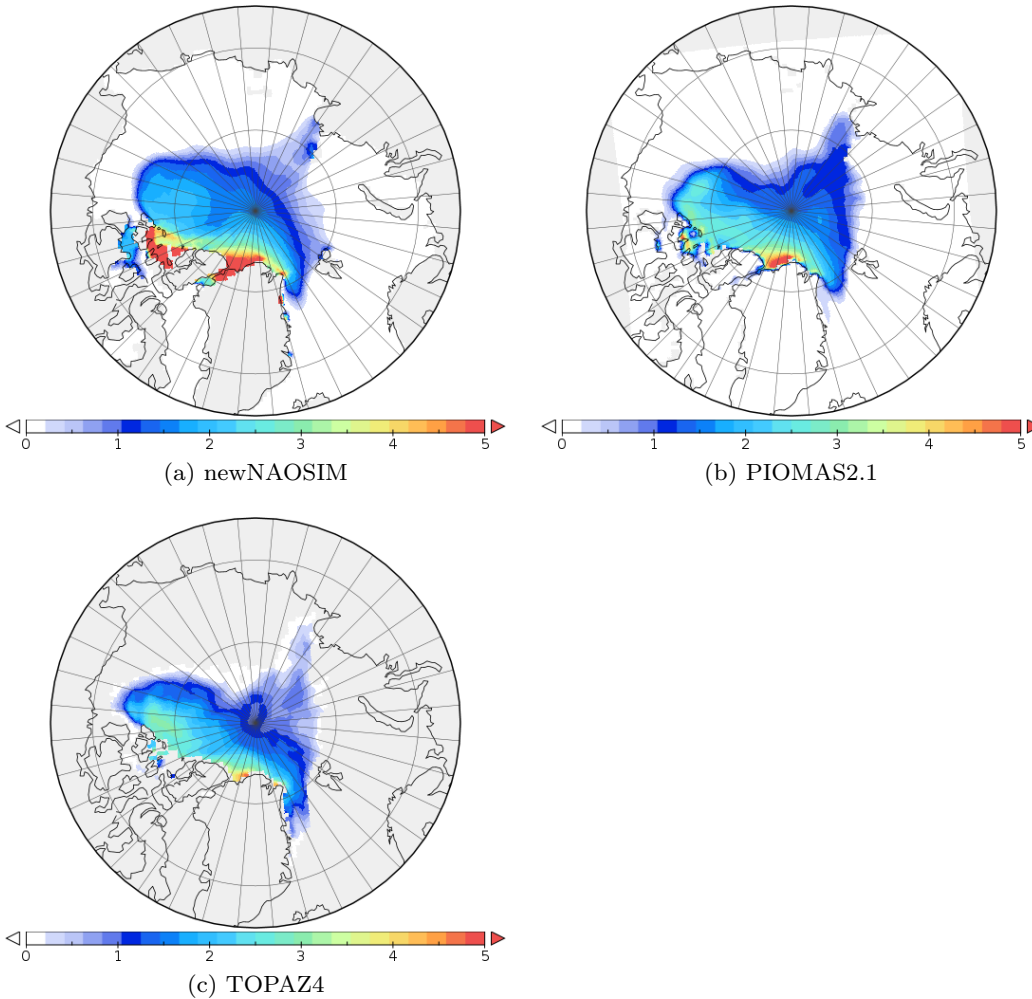


Figure 3: The sea ice thickness [m] September 2007 as simulated by a) newNAOSIM, b) PIOMAS2.1, and c) TOPAZ4.

### 3 Experiments

In this section three different sets of experiments are described (see **Table 2**): The first set performs a straightforward initialisation through simultaneous assimilation of all four data streams described in section 2.2.2. The second set uses all data streams but the ice thickness, and aims at reconstructing ice thickness fields that are consistent with those three data streams and the model. Based on these reconstructed fields a bias correction scheme for CryoSat-2 ice thickness is derived and applied in the final set of experiments. This set of experiments will exhibit a low forecast skill for summer ice concentration, pointing at remaining inconsistencies (despite our thorough calibration of the model). A second set of experiments is used to investigate the mechanism for such inconsistencies: We do this by inferring the evolution of the ice thickness distribution when it is con-

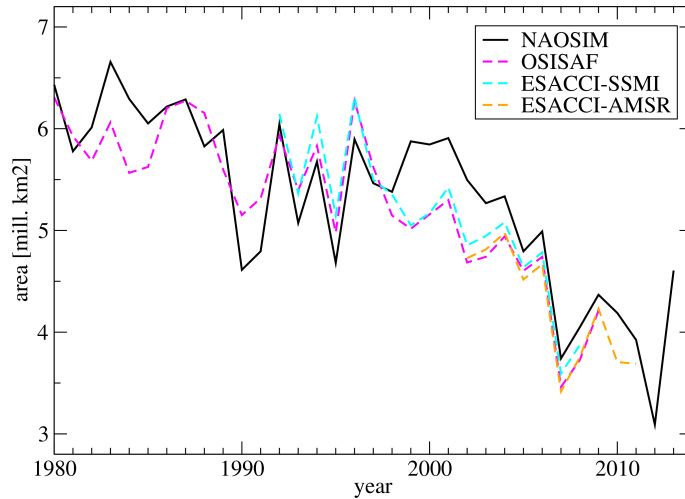


Figure 4: The September sea ice area of newNAOSIM (black) and three estimates based on remotely sensed ice concentration (dashed). OSI SAF (re-processed) and SICCI based on two different sensors (SMMR/SSMI and AMSR, available from [http://icdc.zmaw.de/esa-cci\\_sea-ice-ecv0.html](http://icdc.zmaw.de/esa-cci_sea-ice-ecv0.html)).

assimilation experiment	constraints				
	prior information	daily ice concentration	monthly ice thickness	daily SST	daily snow depth
straightforward	yes	Mar-Apr	Mar-Apr	Mar-Apr	Mar-Apr
reconstruction	yes	Jul-Sep	-	Mar-Sep	Mar-Sep
bias-corrected	yes	Mar-Apr	Mar-Apr	Mar-Apr	Mar-Apr

Table 2: List of sets of experiments performed and the constraints used. Each set of experiments consists of three experiments, one each for the years 2012-2014.

strained only by the other three data streams but not by the CryoSat-2 observations. Based on these “reconstructed” ice thickness fields we will derive a bias correction scheme for CryoSat-2 ice thickness, which is then applied in the final set of experiments.

### 3.1 Straightforward Initialisation

360 We assimilate CryoSat-2 ice thickness (50% retracker threshold), ice concentration, snow depth and SST with uncertainties as described in section 2.2.2. We perform three experiments, one for each of the years for 2012 to 2014, and in each year use a two-month assimilation window from March 1 until April 30. The cost function contribution from CryoSat-2 ice thickness, the data stream in the focus of this study, is based on monthly-mean values, while the contributions from the other 365 data streams are based on daily values. This would result in a substantially lower weight of the

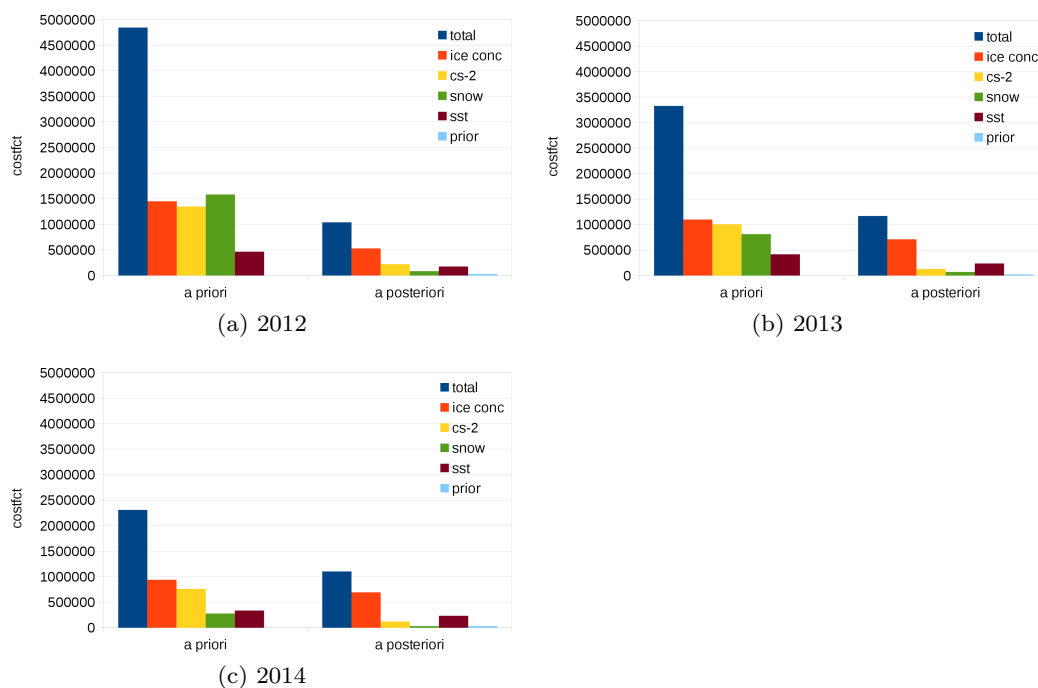


Figure 5: The terms of the cost function before and after the optimization for a) 2012 b) 2013 c) 2014.

ice thickness contribution. We artificially increase its weight by a factor of 180 to ensure that this contribution has the same order of magnitude as the other terms.

In all three experiments, the iterative minimisation procedure of our assimilation system achieves a substantial reduction of the cost function gradient in 50 to 70 iterations. For each experiment, 370 Figure 5 shows the total cost function and the contributions of all four data streams and the prior **information** separately before (a priori) and after the last iteration (a posteriori). The contributions from ice thickness and snow depth are strongly decreased, and for ice concentration and SST the decrease is slightly weaker.

**In the following we use the terms prior simulation, prior run, or simply prior to denote the variables simulated from the a priori control vector and likewise posterior for those simulated 375 from the a posteriori control vector.**

For each experiment, the March ice thickness of CryoSat-2 of the prior run (~~with a priori control vector~~) and the posterior run (~~with a posteriori control vector~~) are shown in Figure 6. The Beaufort Sea, the East Siberian Sea and in the Kara and Laptev Seas exhibit the largest change from prior 380 to posterior. In March 2014, both prior and posterior simulations show (consistent with CryoSat-2) thicker ice north of the Canadian Archipelago and north of Greenland than in 2012 and 2013. With the exception of the area east of Greenland which is of less interest for this study, strong differences between the posterior run and CryoSat-2 are restricted to the area north of Fram Strait towards the

pole and the 2012 experiment. This residual misfit can be traced back to an inconsistency between  
385 observed ice concentration and thickness (and the model): As the simulated ice concentration in  
winter and spring in the Greenland Sea is too high (and, thus, the ice margin too far south) the  
assimilation responds by a reduction of ice thickness north of Fram Strait towards the pole, reflecting  
the pathway of the Transpolar Drift in the model. In other words: the **price** we have to pay for a more  
reliable ice margin is a misfit to the CryoSat-2 ice thickness. Especially in March 2012 CryoSat-2 is  
390 showing very thick ice next to and along the described pathway (Figure 6 a)) which is obviously not  
consistent with the model's ice margin (and ice dynamics).

As we assimilate only data in March and April, the observations for the subsequent months (when  
available) provide independent information that we can use to assess the forecast skill prior and  
posterior to the assimilation. Our skill score is the squared misfit weighted by the reciprocal of  
395 the squared uncertainty (as in ~~the definition of the cost function~~ equation (3), but without the extra  
scaling factor for the ice thickness contribution). For each experiment Figure 7 shows the prior and  
posterior contributions to the misfit per data stream and month from March to December. In all  
experiments, for March and April (i.e. in the assimilation window) the contribution of CryoSat-2 is  
strongly reduced in the posterior run. In November, however, the skill of the posterior run is reduced  
400 for the 2012 and 2013 experiments, and only slightly increased for 2014. The skill for snow depth  
simulation is strongly increased from March to June in 2012 and 2013, for 2014 is was already good  
in the prior. The period from July to September is less relevant, because there is little snow left. The  
skill for SST improves somewhat in March and April.

The posterior ice concentration has an increased skill in March and April. In the subsequent  
405 months the situation is mixed, at least Arctic-wide. We can, however, identify regions of increased  
and reduced skill as is illustrated by Figure 8, which shows the September concentration misfit for  
the prior (row 1) and the posterior (row 2) simulations. For example, the skill in the Beaufort Sea  
and north of the Chukchi plateau is increased, while the skill over the Eurasian basin is decreased.

### 3.2 Reconstruction

410 Our next set of (three) experiments explores the feasibility of inferring an initial ice thickness distri-  
bution on March 1 that is consistent with the summer ice concentration for each of the years 2012  
to 2014. We, hence, use an extended assimilation window from March 1 to September 30 and as-  
similate ice concentration from July to September 30 together with snow depth and SST which we  
assimilate from March to September. We do not use any ice thickness observations. We use the same  
415 control vector as in the straightforward assimilation.

In each experiment the posterior March ice thickness exceeds the CryoSat-2 observations in large  
parts of the Arctic (see Figure 6, rows 3 and 1). Areas with similar values as CryoSat-2 are the  
southern parts of the Beaufort Sea, the Chukchi Plateau, and the Kara and Laptev Seas. Over the  
Eurasian Basin slope except for areas north of the Laptev Sea the posterior ice thickness falls below

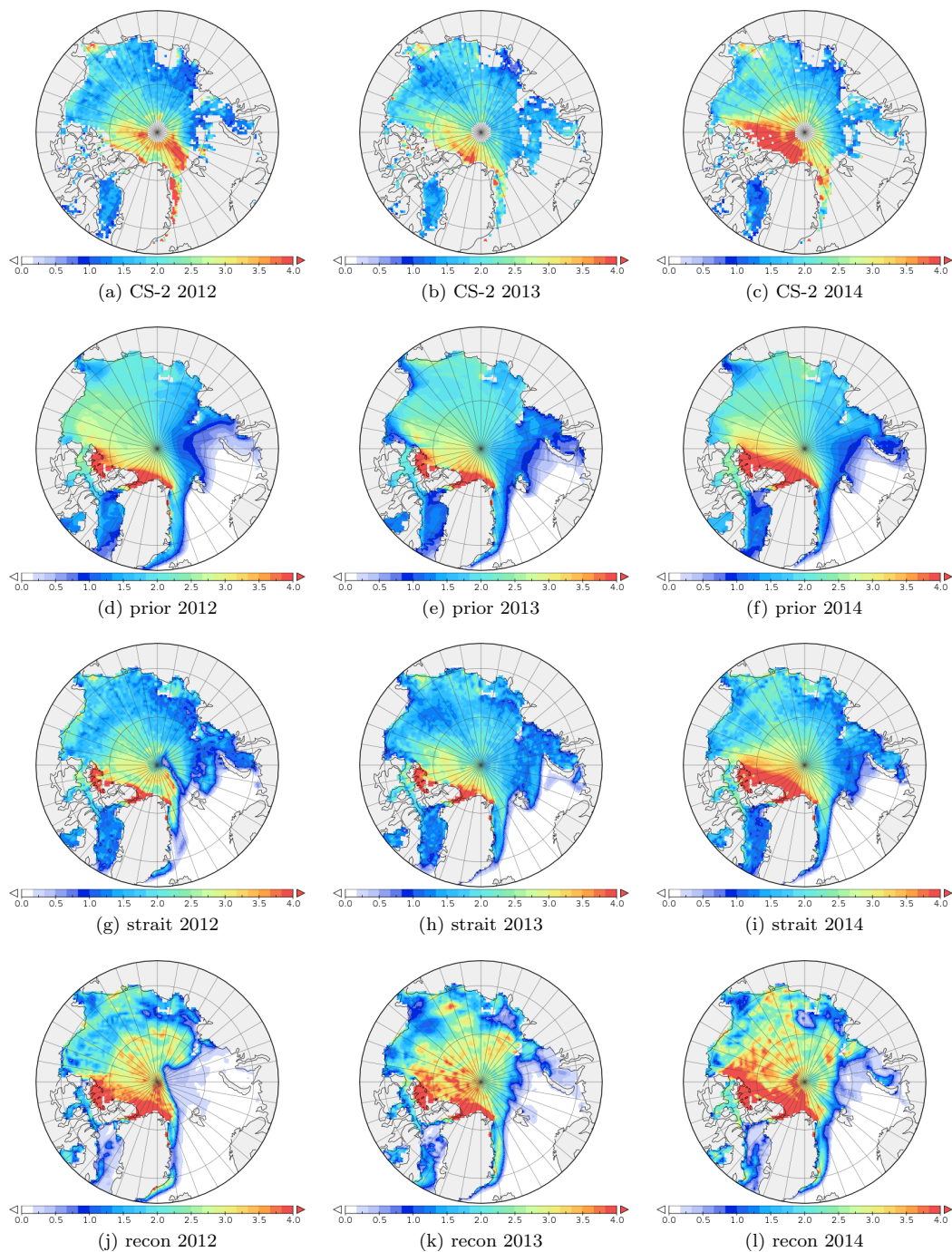


Figure 6: The ice thickness [m] of the CryoSat-2 product (top row); ice thickness of newNAOSIM prior to the assimilation (second row), after the straightforward assimilation (third row), and after the reconstruction (fourth row) for March 2012 (a, d, g, and j)), March 2013 (b, e, h, and k)), and March 2014 (c, f, i, and l)).

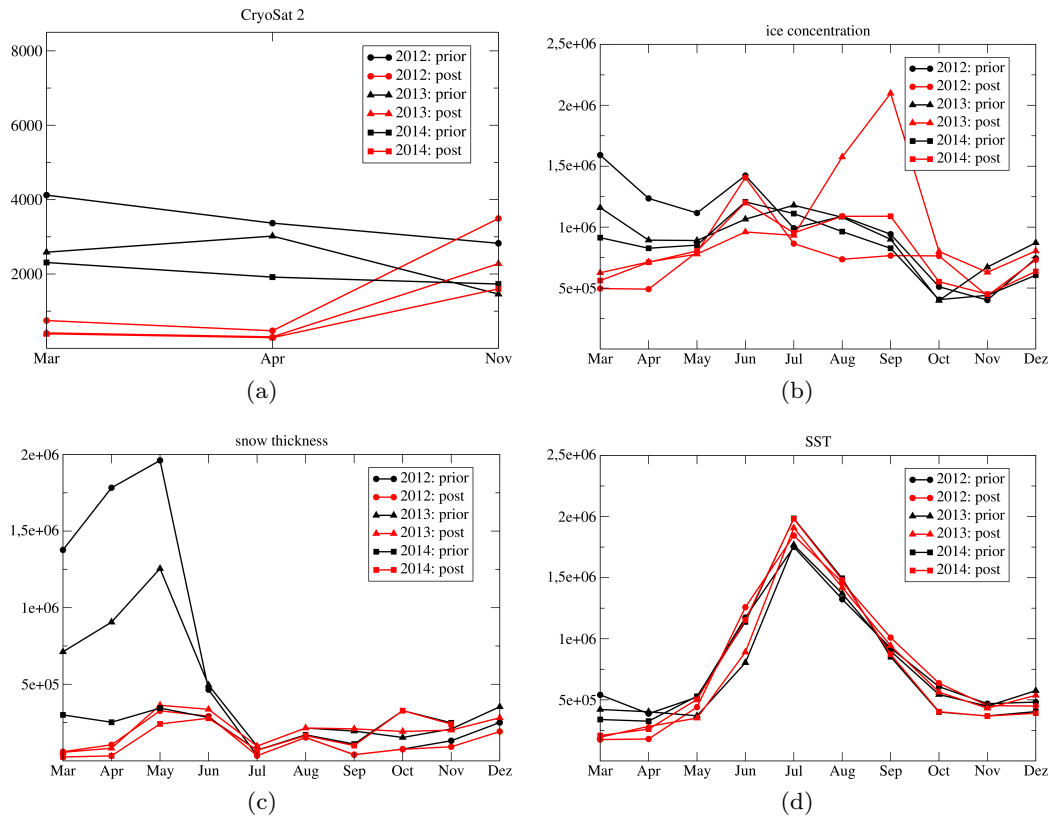


Figure 7: Prior (**black**) and posterior (**red**) misfit (as defined in equation (3)) per data stream and month for a) the CryoSat-2 ice thickness (data are currently only available for March, April and November; not scaled, see text), b) the OSI SAF ice concentration, c) the snow depth (UB), and d) the OSI SAF SST. **The three black (red) lines are representing respectively the three years 2012-2014 and are marked by different symbols (circle: 2012, triangle: 2013, square: 2014).**

420 CryoSat-2. Apparently high ice thickness values are required to match the ice concentration in summer which is shown in row 3 of Figure 8. Note that, compared to the straightforward initialisation experiments here the ice margins are matching. Animations of ice thickness and concentration show that the improved match over the Eurasian Basin slope is caused by increased initial ice thickness north of the Laptev Sea (see row four in Figure 6).

425 We can now compare our skill metrics, i.e. the ~~cost function contributions~~ **contributions to the total misfit (defined in equation (3))** per data stream and month from March to December (Figure 9) with that for the straightforward initialisation (Figure 7) The skill for ice concentration (panel b) is considerably increased from July to September (assimilated) but also from March to June (not assimilated). The skill is, however, already lost in October, probably because of the freezing of sea ice, which is not constrained by any satellite observations of the sea ice. Compared to our run from

430

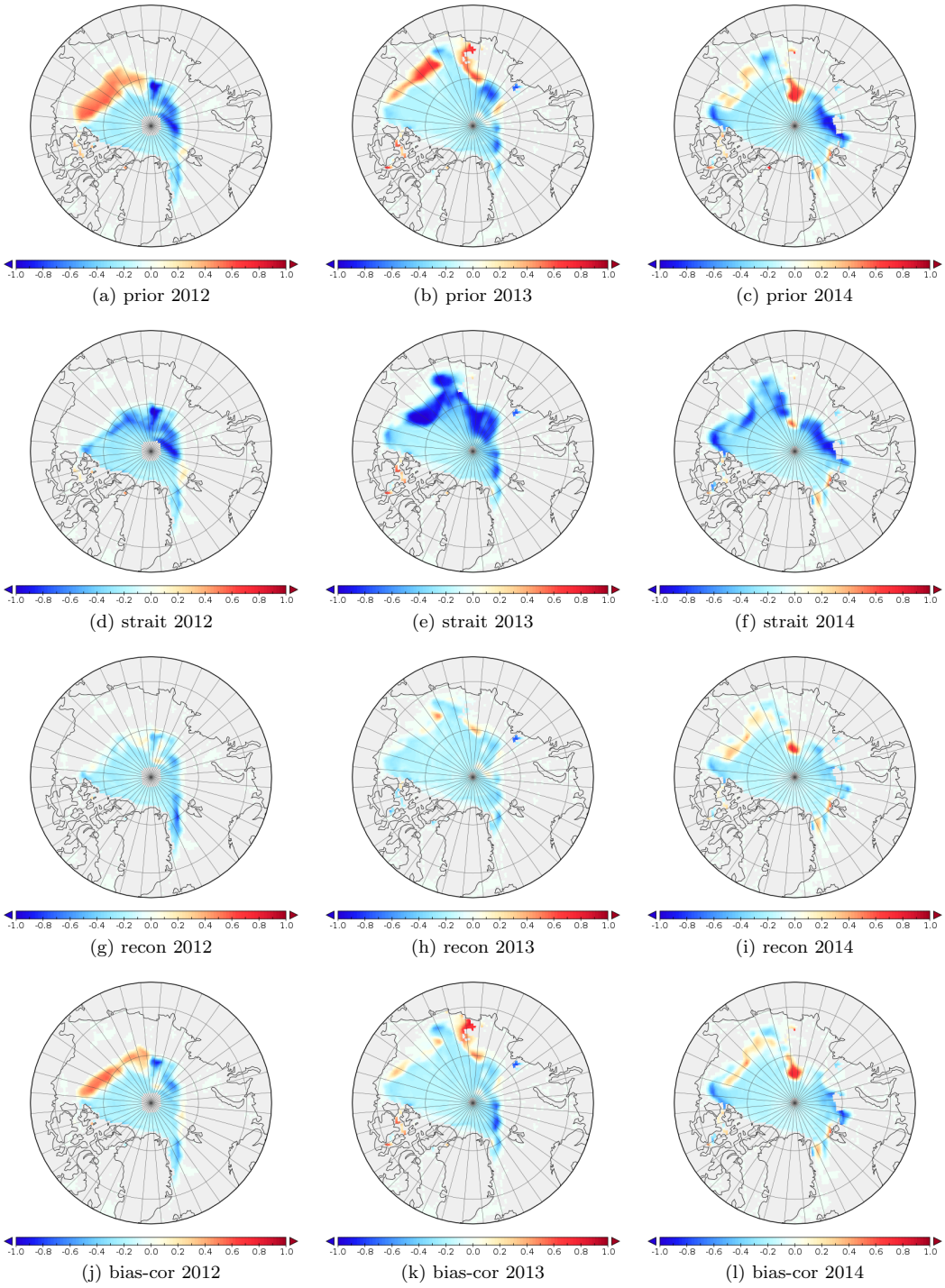


Figure 8: The misfit between simulated and OSI SAF ice concentration prior to (top row), after the straightforward assimilation (second row), after the reconstruction (third row), and after the bias-corrected assimilation (fourth row) and the OSI SAF ice concentration for September 2012 (a, d, g, and j), September 2013 (b, e, h, and k), and September 2014 (c, f, i and l)).

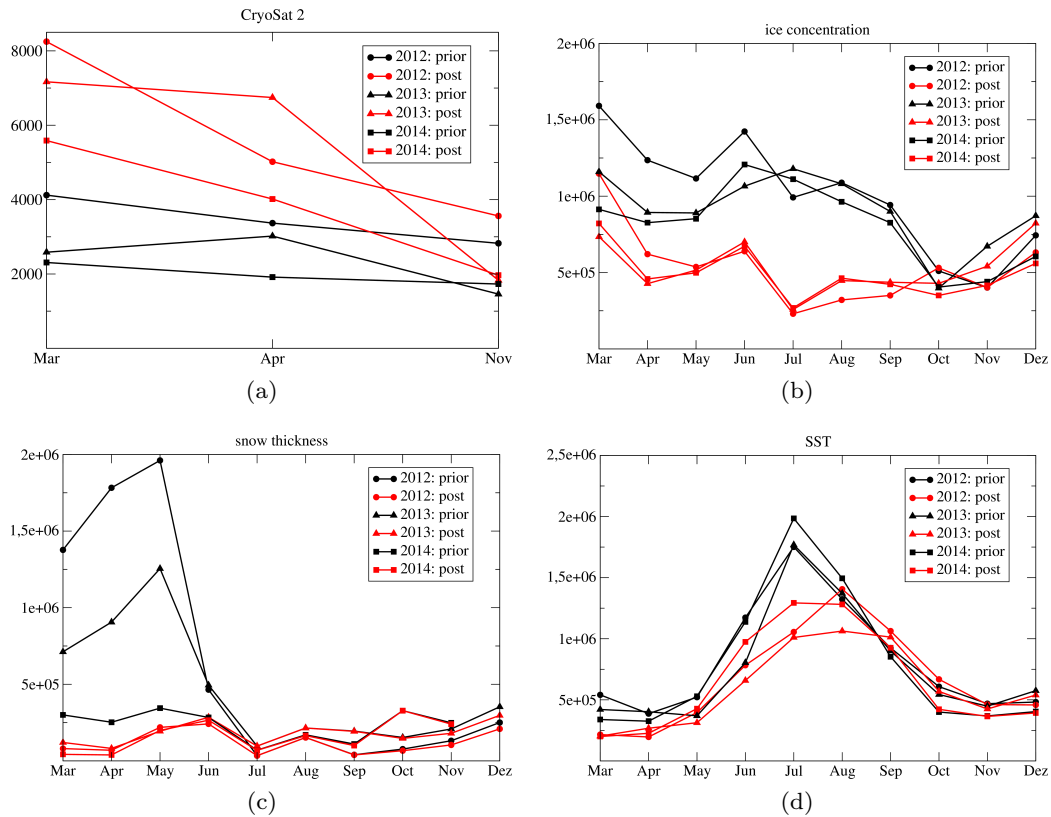


Figure 9: As Figure 7 but for the reconstruction experiment.

the prior initial state, the skill for CryoSat-2 data (panel a) is strongly reduced for March and April but only weakly reduced for November. The skill of snow depth is very similar to that of the straightforward initialisation. The fit to SST shows some improvement from May to August, compared to the prior and to the straightforward assimilation. This is probably an effect of the extended assimilation window, and maybe rather driven by observations of ice concentration than of SST.

### 3.3 Initialisation with Bias Correction

The ratio of the reconstructed and the CryoSat-2 ice thickness shows remarkable similarities of the three years (shown in Figure 10 for March). We use this finding to derive a bias correction procedure: First, we average the ratio fields over the three years from 2012 to 2014 **separately** for March and April (shown in Figure 11 for ~~March in April~~). Second, we multiply the CryoSat-2 ice thickness for March and April by the corresponding ratio fields yielding bias-corrected CryoSat-2 ice thickness fields. Then we repeat the straightforward initialisation (described in section 3.1) with the bias corrected CryoSat-2 fields.

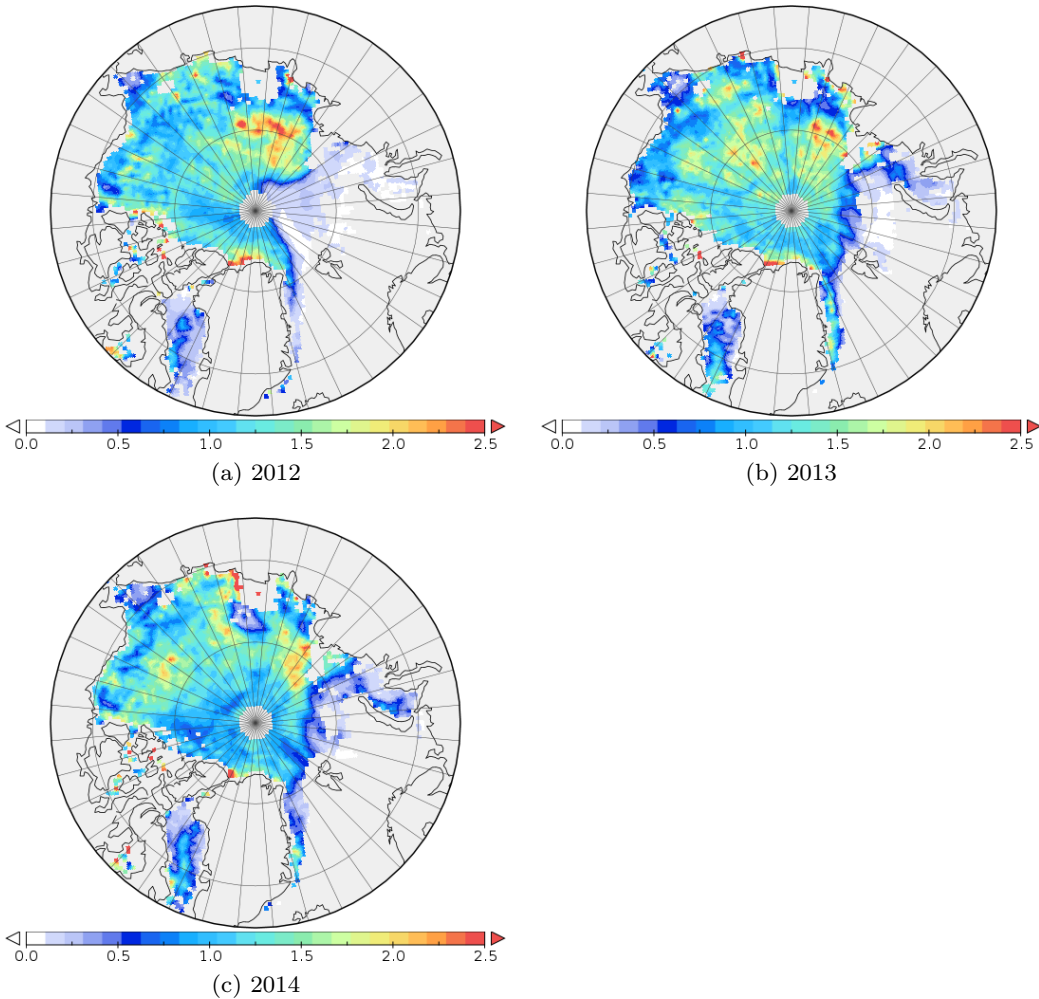


Figure 10: The ratio of the reconstructed and the CryoSat-2 ice thickness a) March 2012, b) March 2013, and c) March 2014.

We note the higher reconstructed ice thickness northeast of Severnaya Zemlya of about a  
 445 factor of two as compared to CryoSat-2 (Figure 11). The model's transpolar drift propagates  
 this increased spring ice thickness towards Fram Strait shifting the summer ice margin further  
 south improving agreement with the observed September ice concentration over the western  
 Nansen basin (compare top and third rows of Figure 8). We also note that this bias correction  
 would also have increased the simulated autumn ice thickness north of Franz Josef's Land  
 450 and thus would have improved the fit to IceSat-JPL data (see Figure 2 panel b). As the two  
 sequential assimilation systems we compared the calibrated model with exhibit the same misfit  
 to IceSat-JPL the bias correction method might have a similar effect for these systems (see  
 Figure 2 panels d and f).

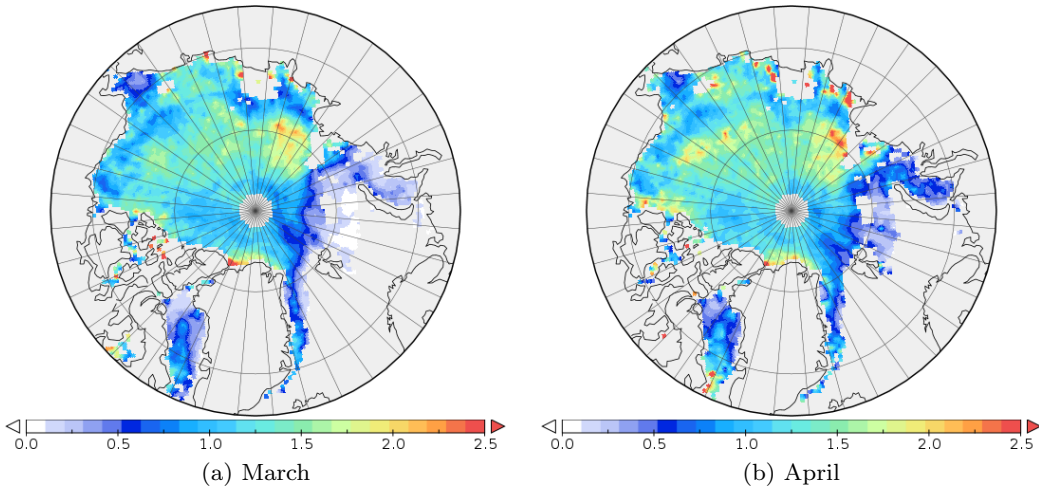


Figure 11: The **three-year mean (2012-2014)** of the ratio of the reconstructed and the CryoSat-2 ice thickness for a) March and b) April.

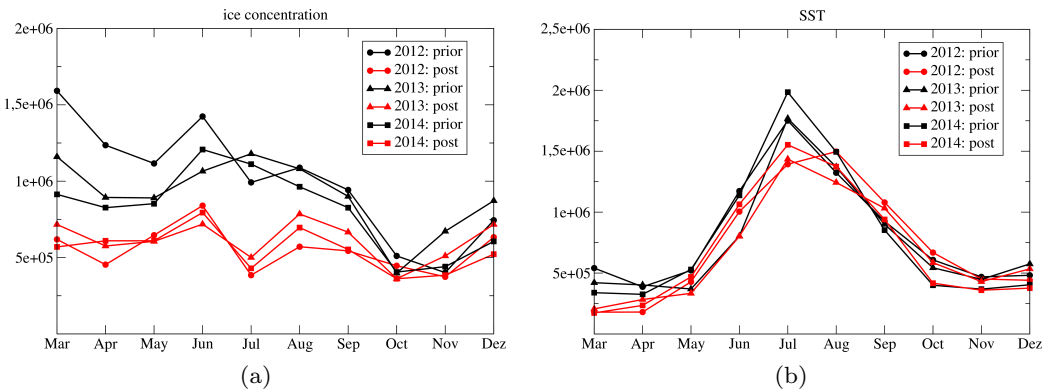


Figure 12: As Figure 7 but for the bias-corrected assimilation experiment. Only the misfit of the ice concentration and SST are shown.

The convergence of the minimisation is similar to that of the straightforward initialisation. The skill of the posterior concentration does, however, show a remarkable improvement until September (Figure 12). The skill for SST is increased from March until July, and for snow depth it is very close to the straightforward initialisation (not shown). The misfit of the ice concentration in September is now strongly reduced for all years (row 4 of Figure 8).

#### 4 Conclusions

AWI's ocean sea ice model NAOSIM has been recalibrated using observations from 1990 to 2008. We restricted the calibration to parameters which control the sea ice dynamics (but also the ocean

dynamics) resulting in a horizontal ice thickness distribution much closer to the ICESat-JPL observations. We described the development of a variational data assimilation system around AWI's ocean sea ice model NAOSIM for seasonal prediction. In its present setup, the scheme uses  
465 several observational data streams over a single two-month assimilation window (March and April) to constrain the initial conditions of the model on March 1. By construction the system enforces consistency between prior information on the initial state (from a preceding model run), all observational data streams and the model equations, which are employed as a hard constraint. Hard constraint means that the evolution of all variables strictly respects the model  
470 equations, for example co-existence of very thick ice and very low ice concentration in the same grid cell and time step will not occur. Our system will inevitably try to correct for errors in the model or the observations by introducing compensating errors in the inferred initial state. It is thus a necessary pre-requisite to eliminate any known biases. In a preparatory step, we, hence, calibrated the model using independent observations over a long time period (1990 to 2008),  
475 namely remotely sensed observations of ice thickness (ICESat-JPL), ice concentration (OSI SAF), and ice drift (OSI SAF and KIMURA).

To limit the computational effort, we restricted the calibration to a sub-set of parameters that, in initial sensitivity studies, showed high impact on the ice conditions. The calibrated model showed a horizontal ice thickness distribution much closer to the ICESat-JPL observations.  
480 A positive bias in the Beaufort Sea and a negative bias over the Eurasian Basin slope were strongly reduced. This is connected to a reduction of the ice drift speeds which are now much closer to the ice drift provided by OSI SAF and KIMURA. The horizontal ice thickness distribution for single events like the September 2007 sea ice minimum is also improved strongly. The time series of September sea ice extent and area are now much closer to the observations. While the standard  
485 uncalibrated model version produces a minimum in extent and area in 1990 which almost reaches the 2007 values, the calibrated model's 1990 simulation is much more realistic. This underlines the importance of a realistic horizontal ice thickness distribution to simulate extreme events correctly. The model is now able to reproduce the minima in 2007 and 2012 although the extent is somewhat overestimated. Also the long-term trend from 1980 to 2014 in extent and area is captured much  
490 better.

In essence the calibrated model matched the observational data within their (partly large) uncertainty ranges. Still it was difficult to assess whether the result of the calibration exercise is sufficient for our objective (bias elimination). What we could do, however, was to compare with  
495 output of two established (sequential) assimilation systems, which also confirmed the success of the calibration. We note that this calibration is, however, limited by the reliability of the available data streams. For example, given the difference in measurement approach (laser vs. radar altimetry), it is not clear, how consistent the ICESat-JPL ice thickness product (used

**for calibration) and the CryoSat-2 product (to be used for the assimilation/forecasting) are. As both products don't overlap in time a direct comparison is not possible.**

500 A subsequent set of data assimilation experiments uses the following four data streams: CryoSat-2 sea ice thickness from AWI, sea ice concentration from OSI SAF, snow depth from University Bremen, and sea **surface** temperature (SST) from OSI SAF. Three assimilation experiments with these four data sets over an assimilation window covering March and April, for each of the years 2012 to 2014, were carried out and a forecast of the summer ice conditions was performed. To  
505 focus on the effect of constraining the initial state of the ocean sea ice system, we assumed to have perfect seasonal atmospheric forecasts providing perfect surface boundary conditions (for a use of this system in operational mode, uncertainty in boundary conditions is handled through an ensemble approach, **see e.g. Kauker et al. (2010)**). It turned out that the assimilation could only improve the summer conditions for some regions. Arctic-wide the forecast **skill** in summer could not be improved  
510 through the use of the sea ice and ocean surface observations in March and April.

~~A second set of experiments was used to construct an initial state that is consistent with the observational data sets except CryoSat-2 over a longer assimilation window from March to September. From this initial state we simulated the posterior ice thickness distribution in March and April. Since this set of experiments made use of the summer ice conditions, we called the inferred posterior ice~~  
515 ~~thickness fields 'reconstructed'. The ratio of this 'reconstructed' and the CryoSat-2 ice thickness fields for March and April is very similar for all three years. This allowed us to develop a bias correction scheme, which scales the CryoSat-2 ice thickness fields by the monthly three-year mean of the above ratio. Then we performed~~ **We took the bad forecast skill as an indication of remaining biases in the system. Guided by biases in the autumn ice thickness simulated by our and the**  
520 **two above mentioned sequential assimilation systems we suspected inconsistencies between the CryoSat-2 data streams and the rest of our assimilation/forecasting system. Until we fully understand and are able to remove the origin(s) of this bias, we needed to devise a strategy for enhancing the forecast skill through correction of this bias. Our procedure is based on a second set of experiments with a longer assimilation window (March to September). We**  
525 **deliberately omitted the CryoSat-2 data stream in the system and constructed an initial state on March 1 that is consistent with the rest of the system. From this initial state we simulated the ice thickness distribution in March and April. Since this set of experiments made use of the summer ice conditions, we called these simulated ice thickness fields 'reconstructed'. As the ratio of this 'reconstructed' and the CryoSat-2 ice thickness fields for March and April is very**  
530 **similar for all three years, our bias correction scheme uses the three-year mean of this ratio field as a point-wise multiplier for the CryoSat-2 product.**

**To investigate the effect of this bias correction procedure we then performed** a third set of assimilation experiments for March and April similar to the first set of experiments but with the bias correction scheme applied to the CryoSat-2 ice thickness. This procedure yields a considerable

535 improvement in forecast skill for sea ice from July to September for all three years. We note that  
our prediction target, namely the summer ice conditions of 2012 to 2014, have entered the assim-  
ilation procedure, because they were used to derive the ice thickness ratio in our bias correction  
scheme. However, the bias correction scheme can now also be applied to years beyond the period  
from 2012 to 2014. One of these applications is the Sea Ice Outlook 2015. **this does not provide**  
540 **a completely independent assessment, because our prediction target, namely the summer ice**  
**conditions of 2012 to 2014, was used in the construction of the bias correction scheme. Future**  
**assimilation/forecast experiments for years beyond the period from 2012 to 2014, will, however,**  
**be completely independent.**

The main recommendation from this study to the ice forecasting community is to try and  
545 eliminate potential biases between the model (including the boundary conditions) and the ob-  
servational data streams by a thorough calibration of the model and examination of the cali-  
bration results with independent information. Such a procedure can only be a first step, as it  
cannot eliminate all sources of bias. Careful inspection of assimilation results for inconsisten-  
cies is thus essential but requires a tedious analysis. The variational data assimilation approach  
550 in the form used here is a powerful basis for detection of inconsistencies and ultimately their  
removal. As an intermediate step bias correction schemes such as the one we constructed for  
assimilation of the CryoSat-2 ice thickness product are helpful for enhancing the forecast skill  
through compensation of model-data inconsistencies. This appears to apply as well to two es-  
tablished sequential assimilation systems (PIOMAS2.1 and TOPAZ4) as they underestimate  
555 the autumn ice thickness in a similar manner as our system.

*Acknowledgements.* This work has been funded by the European Commission through its Seventh Framework  
Programme Research and Technological Development under contract number 265863 (ACCESS) through a  
grant to OASys and FastOpt.

## References

- 560 AMAP: Snow, Water, Ice and Permafrost in the Arctic (SWIPA): Climate Change and the Cryosphere. Arctic  
Monitoring and Assessment Programme (AMAP), 2011.
- Castro-Morales, K., Kauker, F., Losch, M., Hendricks, S., Riemann-Campe, K., and Gerdes, R.: Sensitiv-  
ity of simulated Arctic sea ice to realistic ice thickness distributions and snow parameterizations, *Jour-  
nal of Geophysical Research: Oceans*, 119, 559–571, doi:10.1002/2013JC009342, [http://dx.doi.org/10.1002/](http://dx.doi.org/10.1002/2013JC009342)  
565 2013JC009342, 2014.
- Chevallier, M. and Salas-Mélia, D.: The Role of Sea Ice Thickness Distribution in the Arctic Sea Ice Po-  
tential Predictability: A Diagnostic Approach with a Coupled GCM, *Journal of Climate*, 25, 3025–3038,  
doi:<http://dx.doi.org/10.1175/JCLI-D-11-00209.1>, 2012.
- Chevallier, M., Salas y Melia, D., Voldoire, A., Déqué, M., and Garric, G.: Seasonal Forecasts of the Pan-Arctic  
570 Sea Ice Extent Using a GCM-Based Seasonal, *Journal of Climate*, 26, 6092–6104, doi:10.1175/JCLI-D-12-  
00612.1, 2013.
- Day, J., Hawkins, E., and Rietsche, S.: Will Arctic sea ice thickness initialization improve seasonal forecast  
skill?, *Geophys. Res. Lett.*, doi:10.1002/2014GL061694, 2014.
- Eastwood, S.: Atlantic High Latitude L3 Sea Surface Temperature Product User Manual Version 2.1, Techni-  
575 cal Report, Norwegian Meteorological Institutes, Oslo, Norway, [http://osisaf.met.no/docs/osisaf\\_ss2\\_pum\\_ahl-sst\\_v2p1.pdf](http://osisaf.met.no/docs/osisaf_ss2_pum_ahl-sst_v2p1.pdf), 2011a.
- Eastwood, S.: Validation Report for the Atlantic High Latitude L3 Sea Surface Temperature product Version 1.0,  
Technical Report osi-203, Norwegian Meteorological Institutes, Oslo, Norway, [http://osisaf.met.no/docs/val\\_hlsst\\_n16.pdf](http://osisaf.met.no/docs/val_hlsst_n16.pdf), 2011b.
- 580 Eastwood, S., Jenssen, M., Lavergne, T., Sorensen, A., and Tonboe, R.: EUMETSAT Ocean and Sea Ice Satellite  
Application Facility. Global sea ice concentration reprocessing product (v1.2). Product user manual, Techni-  
cal Report, Norwegian and Danish Meteorological Institutes, Oslo, Norway and Copenhagen, Denmark,  
2015.
- Gerdes, R., Karcher, M. J., Kauker, F., and Schauer, U.: Causes and development of repeated Arctic Ocean  
585 warming events, *Geophysical Research Letters*, 30, n/a–n/a, doi:10.1029/2003GL018080, <http://dx.doi.org/10.1029/2003GL018080>, 1980, 2003.
- Giering, R. and Kaminski, T.: Recipes for Adjoint Code Construction, *ACM Trans. Math. Software*, 24, 437–  
474, 1998.
- Hibler, W.: A dynamic thermodynamic sea ice model, *Journal Geophysical Research*, 9, 815–846, 1979.
- 590 Hibler, W. I. and Bryan, K.: A diagnostic ice-ocean model, *Journal Physical Oceanography*, 17, 987–1015,  
1987.
- Holland, M. M. and Stroeve, J.: Changing seasonal sea ice predictor relationships in a changing Arctic climate,  
*Geophysical Research Letters*, 38, L18 501, doi:10.1029/2011GL049303, 2011.
- Holland, M. M., Bailey, D. A., and Vavrus, S.: Inherent sea ice predictability in the rapidly changing Arctic  
595 environment of the Community Climate System Model, Version 3, *Clim. Dyn.*, 36, 1239–1253, 2010.
- Kaleschke, L., Tian-Kunze, X., Maaß, N., Mäkynen, M., and Drusch, M.: Sea ice thickness retrieval from SMOS  
brightness temperatures during the Arctic freeze-up period, *Geophysical Research Letters*, 39, L05 501,  
doi:10.1029/2012GL050916, 2012.

- Kalnay, E., Kanamitsu, M., Kistler, R., Collins, W., Deaven, D., Gandin, L., Iredell, M. Saha, S., White, G.,  
600 Woollen, J., Zhu, Y., Leetmaa, A., Reynolds, R., Chelliah, M., Ebisuzaki, W., Higgins, W., Janowiak, J.,  
Mo, K., Ropelewski, C., Wang, J., Jenne, R., and Joseph, D.: The NCEP/NCAR 40-year reanalysis project,  
Bulletin of the American meteorological Society, 77, 437–471, 1996.
- Kauker, F., Gerdes, R., Karcher, M., Köberle, C., and Lieser, J.: Variability of Arctic and North Atlantic sea ice:  
A combined analysis of model results and observations from 1978 to 2001, Journal of Geophysical Research  
605 Oceans, 108, 3182, doi:10.1029/2002JC001573, 2003.
- Kauker, F., Kaminski, T., Karcher, M., Giering, R., Gerdes, R., and Voßbeck, M.: Adjoint analysis of the 2007  
all time Arctic sea-ice minimum, J. Geophys. R., p. L03707, doi:10.1029/2008GL036323, <http://www.agu.org/pubs/crossref/2009/2008GL036323.shtml>, 2009.
- Kauker, F., Gerdes, R., Karcher, M., Kaminski, T., Giering, R., and Voßbeck, M.: June 2010 Sea Ice Outlook  
610 - AWI/FastOpt/OASys, Sea Ice Outlook web page, <http://www.arcus.org/search/seaiceoutlook/index.php>,  
2010.
- Kimura, N., Nishimura, A., Tanaka, Y., and Yamaguchi, H.: Influence of winter sea-ice motion on summer ice  
cover in the Arctic, Polar Research, 32, 20 193, doi:<http://dx.doi.org/10.3402/polar.v32i0.20193>, 2013.
- Köberle, C. and Gerdes, R.: Mechanisms determining the variability 2003: Mechanisms determining the vari-  
615 ability of Arctic sea ice conditions and export, J. Clim, 16, 2843–2858, 2003.
- Koenigk, T. and Mikolajewicz, U.: Seasonal to interannual climate predictability in mid and high northern  
latitudes in a global coupled model, Clim. Dyn., 32, 783–798, doi:10.1007/s00382-008-0419-1, 2009.
- Kurtz, N. T., Richter-Menge, J., Farrell, S., Studinger, M., Paden, J., Sonntag, J., and Yungel, J.: IceBridge  
Airborne Survey Data Support Arctic Sea Ice Predictions, EOS, Transactions American Geophysical Union,  
620 94, doi:10.1002/2013eo040001, 2013a.
- Kurtz, N. T., Farrell, S. L., Studinger, M., Galin, N., Harbeck, J. P., Lindsay, R., Onana, V. D., Panzer, B., and  
Sonntag, J. G.: Sea ice thickness, freeboard, and snow depth products from Operation IceBridge airborne  
data, The Cryosphere, 7, 1035–1056, 2013b.
- Kwok, R. and Cunningham, G. F.: ICESat over Arctic sea ice: Estimation of snow depth and ice thickness,  
625 Geophys. Res. Lett., p. C08010, doi:10.1029/2008JC004753, 2008.
- Lavergne, T., Eastwood, S., Teffah, Z., Schyberg, H., and Breivik, L.-A.: Sea ice motion from low-resolution  
satellite sensors: An alternative method and its validation in the Arctic, Journal of Geophysical Research:  
Oceans (1978–2012), 115, C10 032, doi:10.1029/2009JC005958, 2010.
- Lindsay, R., Haas, C., Hendricks, S., Hunkeler, P., Kurtz, N., Paden, J., Panzer, B., Sonntag, J., Yungel, J., and  
630 Zhang, J.: Seasonal forecasts of Arctic sea ice initialized with observations of ice thickness, Geophys. Res.  
Lett., 39, L21 502, doi:10.1029/2012GL053576, 2012.
- Lindsay, R., Wensnahan, M., Schweiger, A., and Zhang, J.: Evaluation of Seven Different Atmospheric Reanal-  
ysis Products in the Arctic, J. Climate, 27, 2588–2606, doi:10.1175/JCLI-D-13-00014.1, 2014.
- Lorenz, E.: Deterministic Nonperiodic Flow, J. Atmos. Sci., 20, 130–141, 1963.
- 635 Markus, T. and Cavalieri, D.: Snow Depth Distribution over Sea Ice in the Southern Ocean from Satellite Passive  
Microwave Data, in: Antarctic Sea Ice: Physical Processes, Interactions and Variability, edited by Jeffries,  
M., no. 74 in Antarctic Research Series, pp. 19–39, American Geophysical Union, AGU, Washington, D.C.,  
1998.

- Massonnet, F., Fichefet, T., and Goosse, H.: Prospects for improved seasonal Arctic sea ice predictions from  
640 multivariate data assimilation, *Ocean Modelling*, 88, 16–25, 2015.
- Nguyen, A. T., Menemenlis, D., and Kwok, R.: Arctic ice ocean simulation with optimized model parameters:  
Approach and assessment, *J. Geophys. Res.*, 116, doi:10.1029/2010JC006573, 2011.
- Parkinson, C., , and Washington, W.: A large-scale numerical model of sea ice, *Journal Geophysical Research*,  
84, 311–337, 1979.
- 645 Ricker, R., Hendricks, S., Helm, V., Skourup, H., and Davidson, M.: Sensitivity of CryoSat-2 Arctic sea-ice  
freeboard and thickness on radar-waveform interpretation, *The Cryosphere*, 8, 1607–1622, doi:10.5194/tc-  
8-1607-2014, 2014.
- Saha, S., Moorthi, S., Wu, X., Wang, J., Nadiga, S., Tripp, P., Behringer, D., Hou, Y., Chuang, H., Iredell,  
M., Ek, M., Meng, J., Yang, R., Peña Mendez, M., van den Dool, H., Zhang, Q., Wang, W., Chen, M.,  
650 and Becker, E.: The NCEP Climate Forecast System Reanalysis, *Bull. Amer. Meteor. Soc.*, 91, 1015–1057,  
doi:http://dx.doi.org/10.1175/2010BAMS3001.1, 2010.
- Saha, S., Moorthi, S., Pan, H., Wu, X., Wang, J., Nadiga, S., Tripp, P., Kistler, R., Woollen, J., Behringer, D.,  
Liu, H., Stokes, D., Grumbine, R., Gayno, G., Wang, J., Hou, Y., Chuang, H., Juang, H., Sela, J., Iredell, M.,  
Treadon, R., Kleist, D., Van Delst, P., Keyser, D., Derber, J., Ek, M., Meng, J., Wei, H., Yang, R., Lord, S.,  
655 van den Dool, H., Kumar, A., Wang, W., Long, C., Chelliah, M., Xue, Y., Huang, B., Schemm, J., Ebisuzaki,  
W., Lin, R., Xie, P., Chen, M., Zhou, S., Higgins, W., Zou, C., Liu, Q., Chen, Y., Han, Y., Cucurull, L.,  
Reynolds, R., Rutledge, G., and Goldberg: The NCEP Climate Forecast System Version 2, *J. Climate*, 27,  
2185–2208, doi:http://dx.doi.org/10.1175/JCLI-D-12-00823.1, 2014.
- Sakov, P., Counillon, F., Bertino, L., Lisæter, K. A., Oke, P. R., and Korablev, A.: TOPAZ4: an ocean-sea ice  
660 data assimilation system for the North Atlantic and Arctic, *Ocean Sciences*, 8, doi:10.5194/os-8-633-2012,  
2012.
- Schweiger, A., Lindsay, D., Zhang, J., Steele, M., and Stern, H.: Uncertainty in modeled arctic sea ice volume,  
*J. Geophys. R.*, 116, C00D06, doi:10.1029/2011JC007084, 2011.
- Semtner, A.: A Model for the Thermodynamic Growth of Sea Ice in Numerical Investigations of Climate,  
665 *Journal of Physical Oceanography*, 6, 379–389, 1976.
- Sigmond, M., Fyfe, J., Flato, G., Khari, V., and Merryfield, W.: Seasonal forecast skill of Arctic sea ice area  
in a dynamical forecast system, *Geophysical Research Letters*, 40, 529–534, 2013.
- Steele, M., Morley, R., and Ermold, W.: PHC: A global ocean hydrography with a high-quality  
Arctic Ocean, *J. Clim.*, 14, 2079–2087, [http://www.scopus.com/scopus/inward/record.url?eid=2-s2.  
670 0-0035324968&partnerID=40&rel=R7.0.0](http://www.scopus.com/scopus/inward/record.url?eid=2-s2.0-0035324968&partnerID=40&rel=R7.0.0), 2001.
- Stroeve, J., Holland, M. M., Meier, W., Scambos, T., and Serreze, M.: Arctic sea ice decline: Faster than forecast,  
*Geophysical research letters*, 34, L09 501, doi:10.1029/2007GL029703, 2007.
- Stroeve, J., Hamilton, L. C., Bitz, C. M., and Blanchard-Wrigglesworth, E.: Predicting September sea ice:  
Ensemble skill of the SEARCH sea ice outlook 2008–2013, *Geophysical Research Letters*, 41, 2411–2418,  
675 2014.
- Sumata, H., Girard-Ardhuin, T. L. F., Kimura, N., Tschudi, M., Kauker, F., Karcher, M., and Gerdes, R.: An inter-  
comparison of Arctic ice drift products to deduce uncertainty estimates, *Journal of Geophysical Research:  
Oceans*, 119, 4887–4921, doi:10.1002/2013JC009724, <http://dx.doi.org/10.1002/2013JC009724>, 2014.

- Sumata, H., Kwok, R., Gerdes, R., Kauker, F., and Karcher, M.: Uncertainty of Arctic summer ice drift  
680 assessed by high-resolution SAR data, *Journal of Geophysical Research: Oceans*, 120, 5285–5301,  
doi:10.1002/2015JC010810, <http://dx.doi.org/10.1002/2015JC010810>, 2015.
- Tarantola, A.: *Inverse Problem Theory and methods for model parameter estimation*, SIAM, Philadelphia, 2005.
- Wang, W., Chen, M., and Kumar, A.: Seasonal Prediction of Arctic Sea Ice Extent from a Coupled Dynamical  
Forecast System, *Monthly Weather Review*, 141, 1375–1394, doi:10.1175/MWR-D-12-00057.1, 2013.
- 685 Wingham, D., Francis, C., Baker, S., Bouzinac, C., Brockley, D., Cullen, R., de Chateau-Thierry, P., Laxon,  
S., Mallow, U., Mavrocordatos, C., Phalippou, L., Ratier, G., Rey, L., Rostan, F., Viau, P., and Wallis, D.:  
CryoSat: A mission to determine the fluctuations in Earth’s land and marine ice fields, *Advances in Space  
Research*, 37, 841–871, doi:10.1016/j.asr.2005.07.027, 2006.
- Yang, Q., Losa, S., Losch, M., Tian-Kunze, X., Nerger, L., Liu, J., Kaleschke, L., and Zhang, Z.: Assimilating  
690 SMOS sea ice thickness into a coupled ice-ocean model using a local SEIK filter, *Journal of Geophysical  
Research: Oceans*, 119, 6680–6692, doi:10.1002/2014JC009963, <http://dx.doi.org/10.1002/2014JC009963>,  
2014.
- Zhang, J. and Rothrock, D. A.: Modeling global sea ice with a thickness and enthalpy distribution model in  
generalized curvilinear coordinates, *Mon. Wea. Rev.*, 131, 845–861, 2003.
- 695 Zhang, J., Steele, M., Lindsay, R., Schweiger, A., and Morison, J.: Ensemble 1-Year predictions of Arctic sea ice  
for the spring and summer of 2008, *Geophysical Research Letters*, 35, L08 502, doi:10.1029/2008GL033244,  
2008.
- Zwally, H., Yi, D., Kwok, R., and Zhao, Y.: ICESat Measurements of Sea Ice Freeboard and Estimates of Sea  
Ice Thickness in the Weddell Sea, *J. Geophys. R.*, 113, C02S15, doi:10.1029/2007JC004284, 2008.